# A Quasi-Lagrangian Vorticity Budget of Composite Cyclone-Anticyclone Couplets Accompanying North American Polar Air Outbreaks

TAI-JEN GEORGE CHEN[1] AND LANCE F. BOSART

*Department of Atmospheric Science, State University of New York at Albany, Albany, NY 12222*

(Manuscript received 25 May 1978, in final form 1 November 1978)

ABSTRACT

A composite cyclone-anticyclone couplet is constructed from four synoptically similar cases of polar air outbreaks into the Caribbean from off the North American continent. A quasi-Lagrangian vorticity budget is then computed from these data for two consecutive 12 h time periods.

The results show that the divergence and twisting terms in the lower troposphere, the horizontal advection term in the middle troposphere, and the horizontal, vertical and system advection in the upper troposphere are of primary importance in generating negative vorticity tendencies in the area toward (from) which the surface anticyclone (cyclone) is moving. In contrast, only the divergence term in the lower troposphere and horizontal advection term in the mid and upper troposphere are primarily responsible for the intensification and movement of the downstream cyclone.

Computations suggest an apparent anticyclonic vorticity source in the mid and upper troposphere and sink in the lower troposphere for the large-scale motions over the anticyclone region with the reverse true for the downstream cyclone region due to subgrid-scale processes.

## 1. Introduction

This paper presents the results of a quasi-Lagrangian vorticity budget investigation for a composite cyclone-anticyclone couplet during a period of North American polar air outbreaks. It should be regarded as an extension of an earlier paper (Chen and Bosart, 1977, hereafter CB) dealing with a kinetic energy budget of the same cyclone-anticyclone couplet.

The reader is referred to CB for the details of the case selection, compositing technique, computational method and overall synoptic situation.

A quasi-Lagrangian coordinate system is employed in this paper such that

$$\frac{\delta}{\delta t_p}=\frac{d}{dt}-(\mathbf{V}_h-\mathbf{C})\cdot\nabla_p-(\omega-\omega_B)\frac{\partial}{\partial p}, \tag{1}$$

where $\delta/\delta t_p$ is the local tendency following the motion of the system, $\mathbf{V}_h$ the horizontal wind velocity, $\mathbf{C}$ the horizontal system velocity and $\omega$ the vertical velocity. The $\omega_B$ represents the vertical motion of the quasi-Lagrangian isobaric coordinate system. For computational convenience, the center of the surface cyclone and anticyclone, respectively, is chosen as the origin of the coordinate system.

The local rate of change of absolute vorticity in a coordinate system centered with respect to the principal surface cyclone and anticyclone can be written as

$$\underset{\text{(G)}}{\frac{\delta\eta}{\delta t_p}}=\underset{\text{(A)}}{-\mathbf{V}_h\cdot\nabla_p\eta}\underset{\text{(B)}}{-\omega\frac{\partial\eta}{\partial p}}\underset{\text{(C)}}{+\mathbf{C}\cdot\nabla_p\eta}\underset{\text{(H)}}{+\omega_B\frac{\partial\eta}{\partial p}}$$

$$\underset{\text{(D)}}{+\eta\frac{\partial\omega}{\partial p}}\underset{\text{(E)}}{-\mathbf{k}\cdot\nabla_p\omega\times\frac{\partial\mathbf{V}_h}{\partial p}}\underset{\text{(F)}}{+F}, \tag{2}$$

where $\eta$ is the absolute vorticity. Terms (2A) and (2B) are horizontal and vertical advection terms; terms (2C) and (2H) are the corresponding advection terms due to the motion of the system; and terms (2D) and (2E) are the divergence and twisting terms. Term (2H) is generally two to three orders of magnitude smaller than the remaining terms in Eq. (2), and is neglected hereafter. Term (2F) represents dissipative and subgrid-scale processes.

A simple centered finite-difference scheme is used to compute all spatial derivatives. The local vorticity tendency with respect to the moving system is taken as the difference of the vorticity between the 12 h synoptic time periods. For physical consistency of the dynamical processes involved in the moving synoptic-scale systems, values for all terms on the right-hand side of Eq. (2) are linearly averaged with the same synoptic time intervals. The dissipation term (2F) is

[1] Present affiliation: Department of Atmospheric Sciences, National Taiwan University, Taipei 107, Republic of China.



0022-4928/79/020185-10$06.50

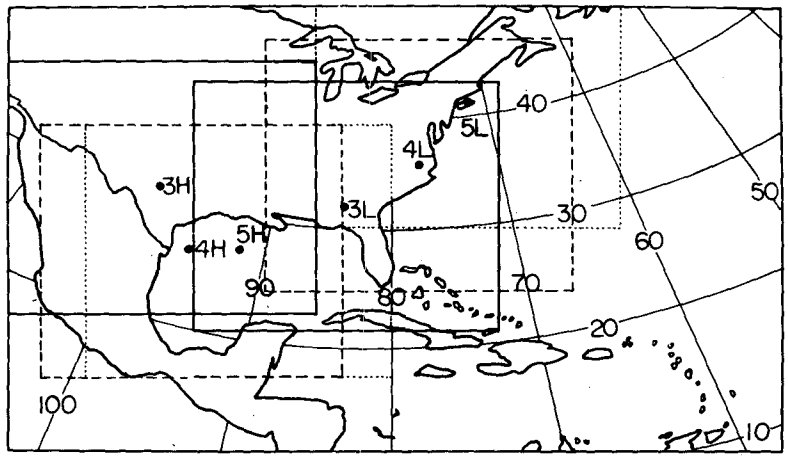


FIG. 1. Limited region moving with the surface anticyclone (H) and cyclone (L). Solid, dashed and dotted lines are boundaries at times 3, 4 and 5, respectively.

then computed as a residual by equating the difference between the left- and right-hand sides of Eq. (2).

Four cases were finally chosen for compositing on the basis of subjectively determined similarities in the surface and tropospheric flow patterns. Each case consisted of eight time periods[2] (times 1–8) at 12 h intervals as follows:

1) 1200 GMT 10 November 1968–0000 GMT 14 November 1968
2) 1200 GMT 7 February 1971–0000 GMT 11 February 1971
3) 0000 GMT 12 February 1971–1200 GMT 15 February 1971
4) 0000 GMT 19 March 1971–1200 GMT 22 March 1971.

For each case the time periods have been relabeled in chronological order as time periods 1–8. The quasi-Lagrangian vorticity budget presented in this paper has been restricted to time periods 3–5, where time period 4 represents the time of the southermost penetration of cold air in terms of the observed 1000–500 mb thickness field. (Refer to CB for details.)

The moving computation domains for the composite cyclone-anticyclone couplet are shown in Fig. 1. The surface position of the cyclone and anticyclone is indicated by the letters L and H, while the numerical prefix indicates the time period.

## 2. Results

### *a. Anticyclone region*

Vertical cross sections through the surface center of relative vorticity and vertical velocity along a line from southwest to northeast for time periods 3, 4 and 5 are shown in Fig. 2. In general, anticyclonic vorticity extends southwestward from the surface center at all levels. At time 3, anticyclonic vorticity maxima are found at 400 mb to the immediate southwest of the surface center and at 850 mb right over the surface center. The lower tropospheric anticyclonic vorticity center moves southwestward while first strengthening and then weakening at times 4 and 5, respectively. A cyclonic vorticity center is situated to the northeast with a maximum value near 300 mb at time 3. It reaches a maximum intensity near 250 mb at time 4 before weakening at time 5.

In general, downward motion prevails over northeastern sections and upward motion over southwestern sections at all levels. At time 3 descent and ascent maxima are 3.8 and $-2.0\ \mu b\ s^{-1}$ at 450 mb, respectively. A doublet pattern is well-developed at time 4 with maxima of $3.4\ \mu b\ s^{-1}$ at 600 mb to the northeast and $-3.0\ \mu b\ s^{-1}$ at 800 mb to the southwest of the surface center. By time 5 broad descent dominates the anticyclone region.

The results obtained by solving Eq. (2) for the anticyclone region are shown in Figs. 3 and 4 for time period 3–4 at the 850 mb level. The divergence term is dominant in the generation of anticyclonic vorticity, especially to the east of the surface center. The twisting term is also important to the south of the surface center in a region of significant horizontal gradient of vertical motion which in part is orographically induced. Overall, the vorticity tendency due to horizontal advection, vertical advection and system advection can only partially compensate the contributions of divergence and twisting to the south and east of the surface center. Thus, the vorticity tendency due to divergence and twisting ensures the southeastward movement of the anticyclone from time 3 to time 4. Fair agreement between the computed and observed local tendencies is seen in Fig. 4. A positive residual or

[2] Each time period is identified as beginning at one time and ending at another. Thus time period 3–4 (or time 3–4) is the 12 h period between time 3 and time 4.

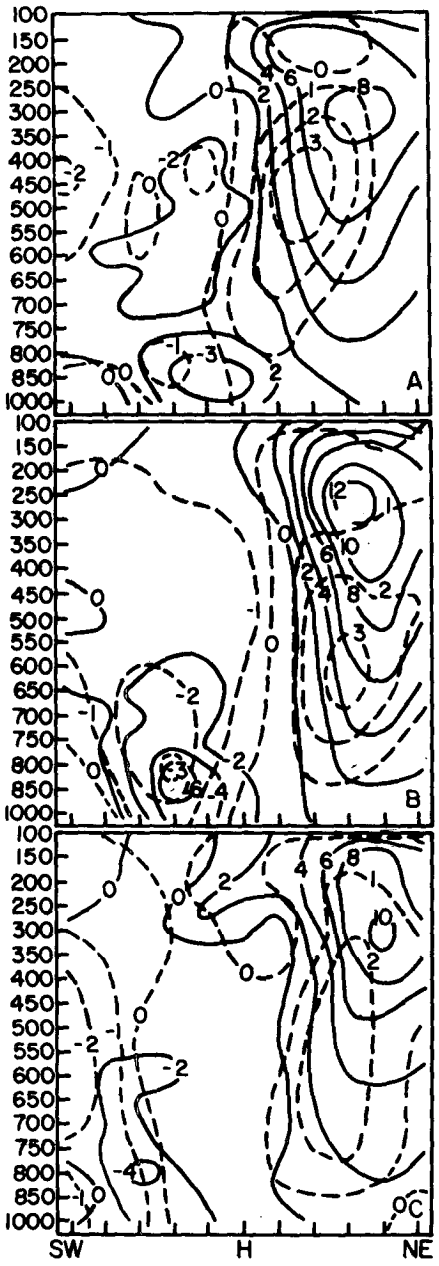


FIG. 2. Vertical cross section of relative vorticity (solid lines, $\times 10^{-5}$ s$^{-1}$) and vertical velocity (dashed lines, $\times 1$ $\mu$b s$^{-1}$), respectively, from southwest (SW) to northeast (NE) across the surface anticyclone center (H) for time 3(A), time 4(B) and time 5(C). The grid spacing on the abscissa is ~150 km.

apparent anticyclonic vorticity sink is obtained in the immediate vicinity of the surface center.

The results also indicate that both the magnitudes and patterns of the different terms for time 4–5 (not shown) are quite similar to those of the previous period in general. The divergence term is even more dominant with the maximum anticyclonic vorticity tendency located to the northeast of the surface center, suggesting a northeastward movement of the surface anticyclone

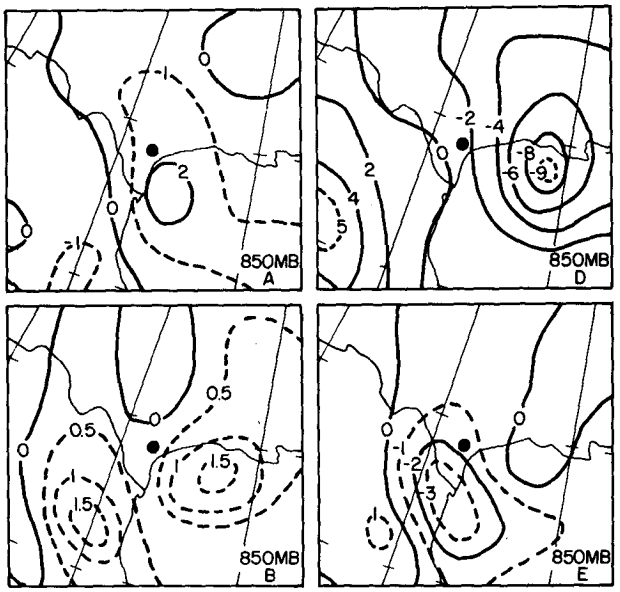


FIG. 3. 850 mb vorticity budget for time 3 to time 4 in units of $10^{-5}$ s$^{-1}$ (12 h)$^{-1}$ due to (A) horizontal advection, (B) vertical advection, (D) divergence and (E) twisting. Anticyclone center is denoted by the solid circle. The letters correspond to the terms indicated in Eq. (2).

after time 5 as observed. The twisting term also decreases in magnitude somewhat but it is still an important mechanism to the southwest of the surface center where the maximum gradient of vertical velocity is found.

Figs. 5 and 6 show the vorticity budget terms at 500 mb for time 3–4. Anticyclonic vorticity advection dominates most of the area in the eastern sector with

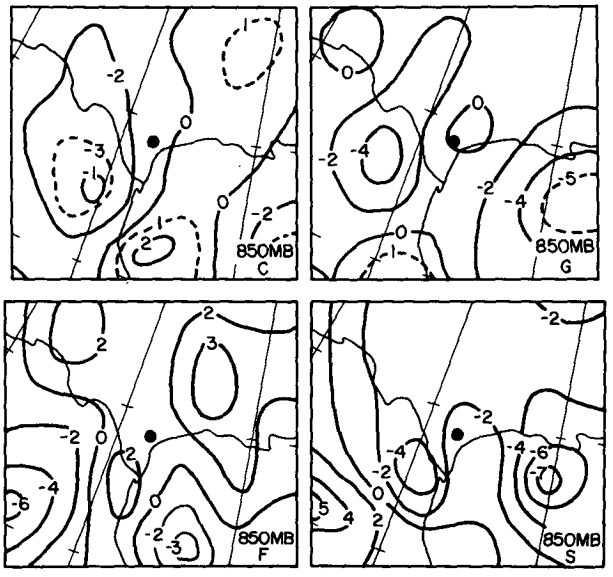


FIG. 4. As in Fig. 3 except for (C) horizontal system advection, (F) residual, (G) observed local tendency and (S) computed local tendency excluding the residual term.

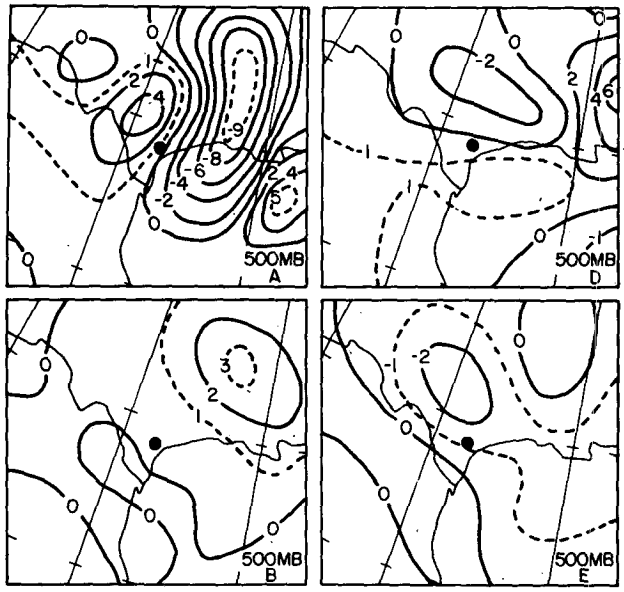


FIG. 5. As in Fig. 3 except for 500 mb.

a maximum value of $-10.0 \times 10^{-5}$ s$^{-1}$ (12 h)$^{-1}$ to the northeast of the surface center, whereas weaker cyclonic vorticity advection prevails elsewhere. Compensation is evident among the remaining terms, especially to the northeast of the surface center. Again, agreement between the computed and observed vorticity tendencies is fair with a large negative residual or apparent anticyclonic vorticity source located to the southeast of the surface center. The patterns of the budget terms for time 4–5 (not shown) are quite similar to those of the time 3–4. Horizontal anticyclonic vorticity advection is most pronounced northeast of the surface center, a clue to the upcoming recurvature of the surface

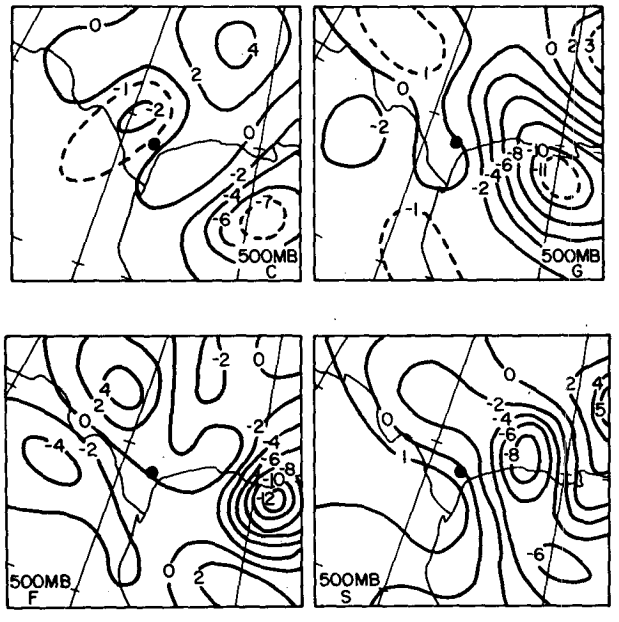


FIG. 6. As in Fig. 4 except for 500 mb.

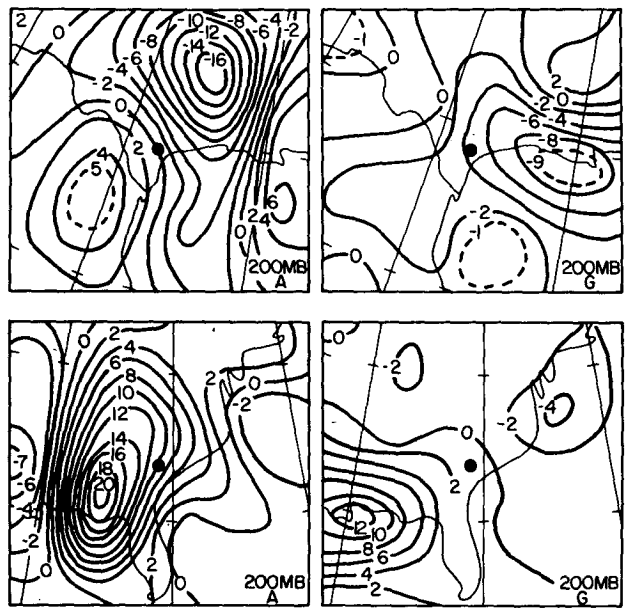


FIG. 7. 200 mb vorticity budget for time 3 to time 4 in units of $10^{-5}$ s$^{-1}$ (12 h)$^{-1}$ due to (A) horizontal advection, (G) observed local tendency for the anticyclone region (top row) and the same terms for the cyclone region (bottom row). Solid dots locate anticyclone and cyclone center, respectively.

anticyclone. Only the horizontal advection and local tendency terms at 200 mb for time 3–4 are shown in Fig. 7. The horizontal advection term and divergence term (not shown) are major contributors, but are of opposite sign almost everywhere over the domain with the former dominant. The residual term (not shown) is also negative at 200 mb for time 3–4 with an area averaged value comparable to 500 mb as can be seen from Fig. 8.

Fig. 8 shows the vertical profiles of the budget terms averaged over the entire $11 \times 11$ computational domain. For time 3–4, the local vorticity tendency (G) and the system advection terms (C) are nearly constant at all levels. Anticyclonic vorticity is generated due to divergence term below 600 mb, whereas the reverse is true above this level. The vorticity tendency due to twisting and vertical advection is of opposite sign and comparable magnitude while the negative vorticity tendency due to advection is most evident in the upper troposphere. A positive residual or apparent anticyclonic vorticity sink is then obtained in the lower troposphere below 700 mb with a negative residual or apparent anticyclonic vorticity source above this level.

In the following time period the composite anticyclone begins to weaken and turn northeastward. This is confirmed from time 4–5 of Fig. 8 which shows very weak cyclonic vorticity tendency averaged over the anticyclone domain. This change is accompanied by a lessening of the overall anticyclonic tendency due to horizontal advection and the development of a very weak negative residual in the 550–350 mb layer.

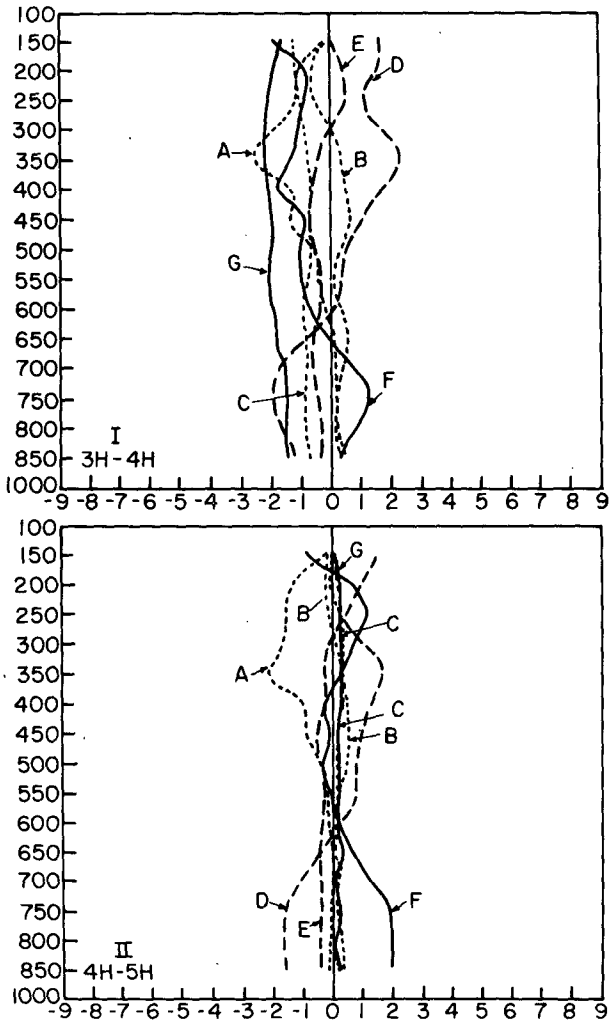


FIG. 8. Vertical profiles of vorticity budget terms in units of $10^{-5}$ s$^{-1}$ (12 h)$^{-1}$ averaged over the 11×11 anticyclone computational domain for time 3 to time 4 (I) and time 4 to time 5 (II). Letters correspond with the terms indicated in Figs. 3 and 4.

### *b. Cyclone region*

Vertical cross sections of relative vorticity and vertical velocity along a line from northwest to southeast and passing through the surface center are shown in Fig. 9 for times 3, 4 and 5. In general, cyclonic vorticity extends from the northwest to the immediate southeast of the surface center at all levels. A noticeable decrease in the tilt of the vertical axis of maximum relative vorticity as a function of time is evident as would be expected for a deepening cyclone. The axis of maximum cyclonic vorticity extends downward and southeastward toward the surface cyclone center with cyclonic vorticity increasing in the lower troposphere. Note the increase in anticyclonic vorticity in the upper troposphere in the flanking ridge to the southeast of the cyclone center such that the maximum horizontal vorticity gradient lies above this center with peak intensity at time period 4.

Most of the area in the vicinity of the surface center is occupied by upward motion at time 3. Downward motion is observed mainly to the northwest in the mid and lower troposphere. At time 4, upward motion intensifies and becomes better organized at all levels in the vicinity of the surface center with a value of $-5.6$ $\mu$b s$^{-1}$ at 500 mb. By time 5, upward motion has decreased in intensity but expanded in horizontal extent.

Figs. 10 and 11 show the vorticity budget terms at

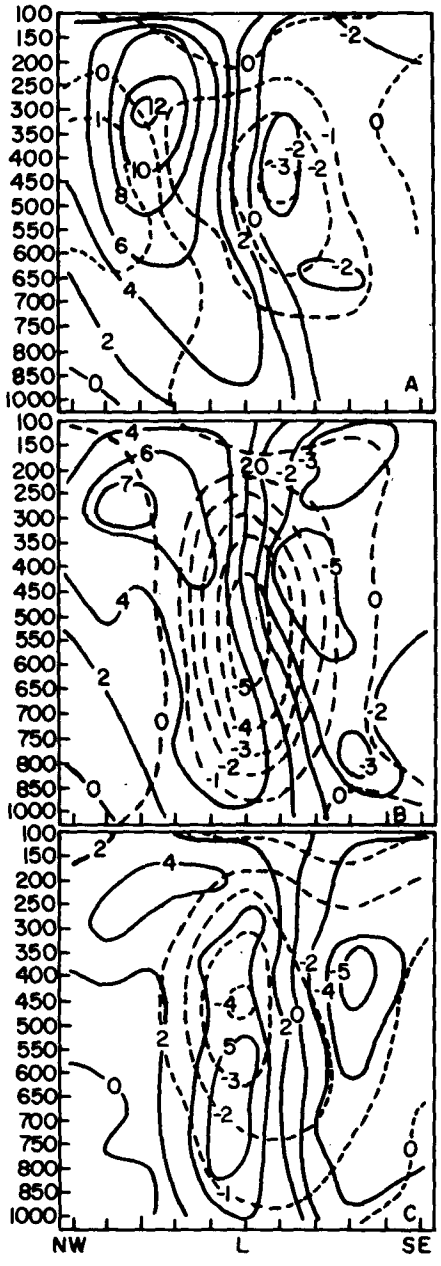


FIG. 9. As in Fig. 2 except for the cyclone region.

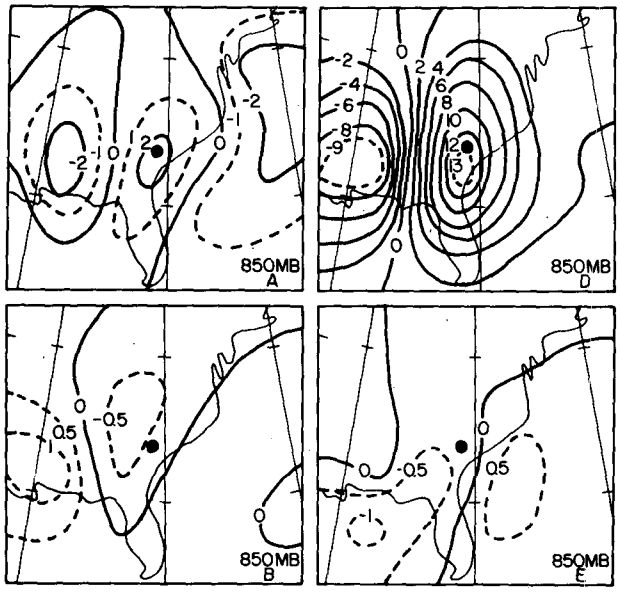


FIG. 10. As in Fig. 3 except for the cyclone region.

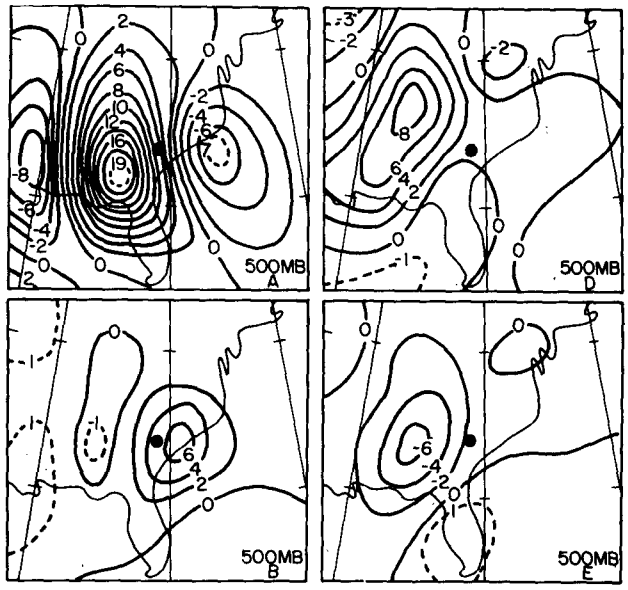


FIG. 12. As in Fig. 5 except for the cyclone region.

850 mb over the surface cyclone for time 3–4. The divergence term is of major importance and is characterized by a doublet pattern. The positive tendency due to this term covers the eastern sector and spreads westward with a maximum value of $13.2 \times 10^{-5}$ s$^{-1}$ (12 h)$^{-1}$ to the immediate south of the surface center. The expected system advection doublet by definition is also evident for the system advection term with a sign reversal as compared to the divergence term in most areas. The vertical advection and twisting terms are of comparable but small magnitude. The cyclonic vorticity tendency due to horizontal advection and the divergence term in the immediate vicinity of the surface center is only partially compensated by the sum of the remaining terms. While the observed local vorticity tendency is positive during this period over most of the area of interest, it is considerably less than the computed tendency in the vicinity of the cyclone center. A large negative residual or apparent cyclonic vorticity sink is then required to bring the budget into balance.

The distribution of vorticity tendencies for time 4–5 (not shown) is quite similar to that for times 3–4 at 850 mb. Overall generation of cyclonic vorticity due to convergence is nearly doubled to the immediate south of surface center while the local cyclonic tendency increases over most of the area with a maximum of $6.2 \times 10^{-5}$ s$^{-1}$ (12 h)$^{-1}$ to the south-southwest of the surface center.

Figs. 12 and 13 show the results of 500 mb for time 3–4. In general, the vertical advection, twisting and divergence terms are comparable in magnitude, although smaller than the horizontal advection and system advection terms. Cyclonic vorticity advection prevails in the vicinity of the surface center with a maximum value of $19.0 \times 10^{-5}$ s$^{-1}$ (12 h)$^{-1}$ to the immediate southwest. The system advection term has a pattern similar to the horizontal advection term but with a sign reversal. The positive vorticity tendency due to the vertical advection term to the southeast of the surface center is apparently due to the upward transport of higher cyclonic vorticity air from below (Fig. 9). The overall computed local tendency is in fair agreement with the observed tendency with a maximum found to the southwest of the surface center. A generally negative residual or apparent cyclonic vorticity sink is then seen near the cyclone center.

Little change is evident in the overall 500 mb tendency patterns for time 4–5 (not shown). The magnitude of the cyclonic vorticity advection tendency increases while rotating counterclockwise with respect

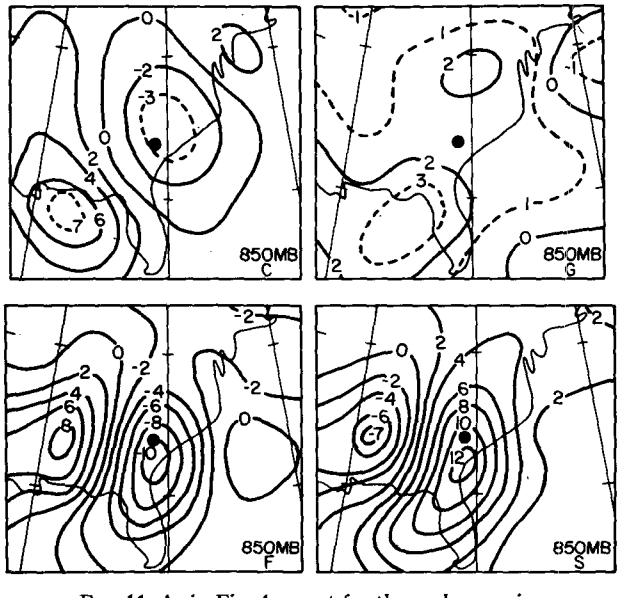


FIG. 11. As in Fig. 4 except for the cyclone region.

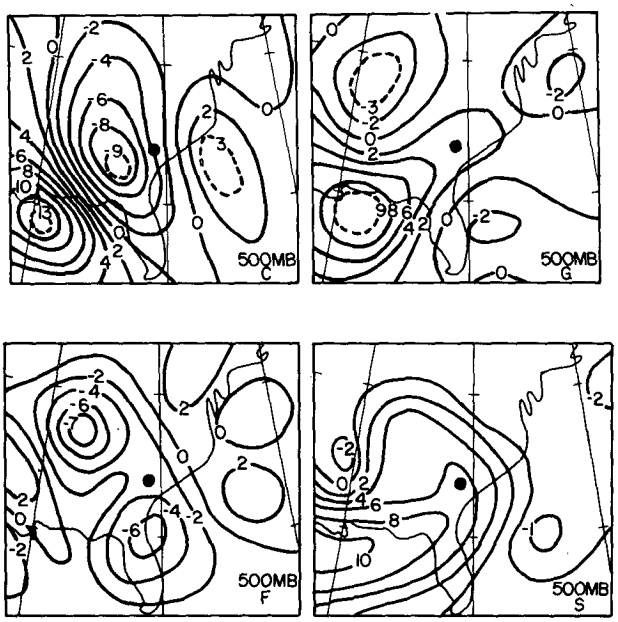


FIG. 13. As in Fig. 6 except for the cyclone region.

to the surface cyclone center as sould be expected for an intensifying system. At 200 mb powerful cyclonic vorticity advection to the southwest of the cyclone center dominates all other computed tendency terms (Fig. 7).

These results are summarized in Fig. 14 as vertical profiles of the various budget terms averaged over the entire $11 \times 11$ cyclone volume. Divergence effects generate cyclonic vorticity below 350 mb while destroying it above this level for time 3–4. Surface cyclogenesis and the intensification of the upper level trough are indicated by the positive local tendency at all levels. The twisting and vertical advection terms are rather important in the mid and lower troposphere, and are of opposite sign. The vorticity tendency due to horizontal advection, vertical advection and system advection terms are weakly positive at almost all levels. Consequently, a negative residual or apparent vorticity sink is obtained below 300 mb with a positive residual or apparent vorticity source above that level.

In the following 12 h (time 4–5) the residual term becomes more positive in the upper troposphere and changes sign to positive in the mid-troposphere. The residual term remains negative in the lower troposphere. During this period cyclogenesis continued as can be seen from the vorticity tendency and divergence profiles Likewise the area averaged upward increase in cyclonic vorticity advection is consistent with a deepening cyclone.

### 3. Error analysis

An error analysis procedure based on the method of Kurihara (1961) was employed for the vorticity budget results. Computational details and a more complete discussion of the method can be found in CB. In general the error bounds range from 10 to 50% with the major tendency terms more reliable than the minor tendency terms at all levels. The range of values is thus somewhat less than for the previous kinetic energy budget results. The residual term, however, is quite reliable in both sign and magnitude.

A disadvantage to such an error analysis scheme is the assumption that the data used to compute the various terms in the vorticity equation are independent. Thus the indicated upper error bounds may be underestimates. In the absence of any other direct error checks (e.g., a vorticity budget study of an innocuous case to establish possible error bounds on the residual term) appeal must be made to indirect evidence. The data set employed here is identical to that used in our previous kinetic energy study of the same composite cyclone-angicyclone couplet. The results from this paper and CB are consistent with those of other investigators such as Kung (1977), Kung and Baker

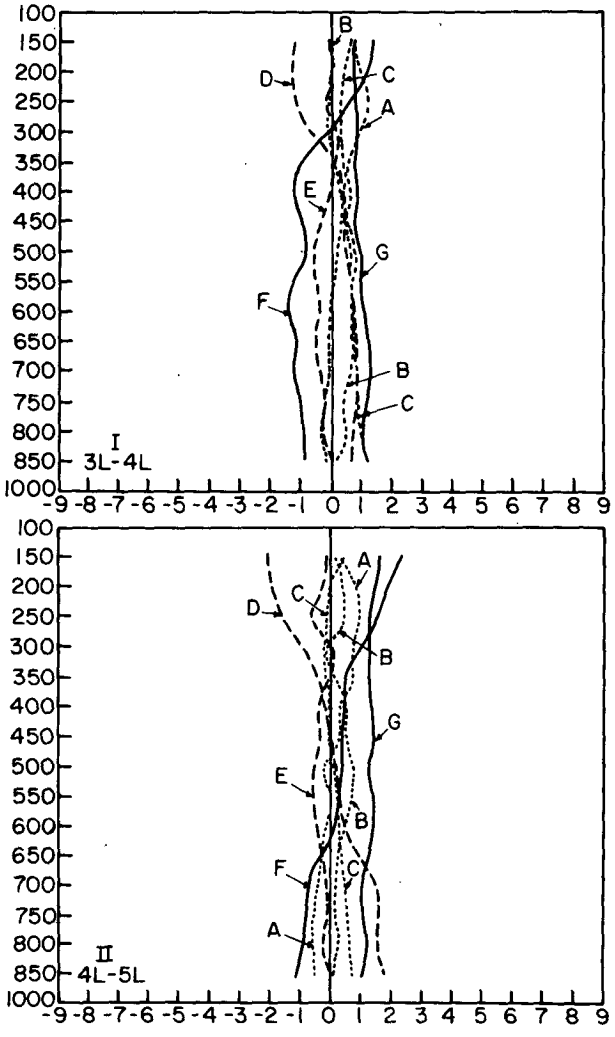


FIG. 14. As in Fig. 8 except for the cyclone region.

TABLE 1. Vorticity budget terms [$10^{-5}$ s$^{-1}$ (12 h)$^{-1}$] at upstream point X and downstream point Y for the surface anticyclone from time 3 to time 4.

| Level | A $-\mathbf{V}_h\cdot\nabla_p\eta$ | | B $-\omega(\partial\eta/\partial p)$ | | C $\mathbf{C}\cdot\nabla_p\eta$ | | D $\eta\,\partial\omega/\partial p$ | | E $-\mathbf{k}\cdot\nabla_p\omega x(\partial\mathbf{V}_h/\partial p)$ | | G $\delta\eta/\delta t_p$ | | A+B+C+D+E | |
|---|---|---|---|---|---|---|---|---|---|---|---|---|---|---|
| (mb) | X | Y | X | Y | X | Y | X | Y | X | Y | X | Y | X | Y |
| 300 | 0.3 | −5.3 | −0.3 | 1.6 | −1.0 | 0.3 | −0.0 | −2.2 | −1.3 | −2.1 | 1.0 | −2.9 | −2.4 | −7.8 |
| 590 | 3.8 | −2.4 | 0.3 | 0.0 | −1.6 | 0.6 | −1.8 | 1.8 | −2.3 | −0.2 | −0.1 | −1.0 | −1.7 | −0.2 |
| 850 | 1.2 | 2.2 | −0.1 | 0.7 | −1.7 | 0.1 | −1.1 | −1.9 | −1.0 | −2.2 | −1.8 | −0.6 | −2.6 | −1.1 |

(1975), Vincent *et al.* (1974), Smith (1973) and Holopainen (1963, 1973) who have made extensive studies of the cyclone environment.

## 4. Discussion

Tables 1 and 2 summarize the vorticity budget results for positions upstream and downstream of the surface cyclone and anticyclone, respectively, at 300, 500 and 850 mb for time period 3–4. Point X represents the position from which the surface center has moved, while point Y indicates the location toward which the surface center is moving. The distance between X and Y is ~650 km (750 km) for the surface anticyclone (cyclone). The numbers in the tables represent the arithmetic mean of the four grid points surrounding locations X and Y.

At 850 mb primary anticyclonic vorticity generation downstream from the surface anticyclone arises from the divergence and twisting terms whereas horizontal advection is the primary destructive mechanism. Downstream of the surface cyclone the divergence term is dominant in the generation of cyclonic vorticity with the advection and twisting terms an order of magnitude smaller. Significant upstream vorticity generation due to divergence is also seen for the surface cyclone as time period 3–4 represents a period of sustained intensification at all tropospheric levels in this region. Little change was noted for time 4–5 (not shown) at the 850 mb level except that the twisting term was not as significant in the generation of anticyclonic vorticity downstream of the surface cyclone. Cross-stream horizontal vertical motion gradients were reduced as the anticyclone reached the southernmost extent before beginning to weaken and turn northeastward.

Horizontal vorticity advection was the dominant producer of anticyclonic vorticity downstream of the surface anticyclone position at 500 mb for both time 3–4 and time 4–5 (not shown). A very weak anticyclonic vorticity tendency was exhibited by the twisting term whereas the divergence term acted in the opposite sense. Upstream of the surface anticyclone the roles of the advection and divergence terms were reduced at 500 mb.

Powerful cyclonic vorticity advection, partially offset by system advection and twisting effects, is evident upstream from the surface cyclone at 500 mb. Little effect is seen from the divergence term. Downstream from the surface cyclone the computed tendencies are considerably weaker with vorticity generation primarily due to vertical advection, divergence and system advection. The pattern holds true for time 4–5 (not shown) except that the twisting term becomes inportant as a secondary source of cyclonic vorticity as the surface cyclone continues to intensify.

At 300 mb the anticyclonic vorticity tendency downstream of the surface anticyclone is produced primarily by advection with the divergence and twisting terms acting as secondary sources.

Overall, the anticyclone region features destruction (production) of anticyclonic vorticity below (above) 650 mb for both time periods (recall Fig. 8). This profile is somewhat similar to that found by Reed and Johnson (1974) for a composite ridge based on three months of easterly wave observations in the tropical western Pacific. The apparent anticyclonic vorticity sinks and sources act to reduce the vorticity changes being produced by, e.g., synoptic-scale convergence. Vertical transport of vorticity due to convective-scale motions as suggested by Holton and Colton (1972) is unlikely to be of significance here due to the broad descent and corresponding absence of convection. Consequently, a subgrid-scale exchange process is required to create anticyclonic vorticity in the mid and

TABLE 2. As in Table 1 except for the surface cyclone from time 3 to time 4.

| Level | A $-\mathbf{V}_h\cdot\nabla_p\eta$ | | B $-\omega(\partial\eta/\partial p)$ | | C $\mathbf{C}\cdot\nabla_p\eta$ | | D $\eta\,\partial\omega/\partial p$ | | E $-\mathbf{k}\cdot\nabla_p\omega x(\partial\mathbf{V}_h/\partial p)$ | | G $\delta\eta/\delta t_p$ | | A+B+C+D+E | |
|---|---|---|---|---|---|---|---|---|---|---|---|---|---|---|
| (mb) | X | Y | X | Y | X | Y | X | Y | X | Y | X | Y | X | Y |
| 300 | 23.7 | 1.2 | 0.4 | −1.2 | −6.2 | −1.8 | −11.5 | −5.1 | 0.2 | −0.4 | 5.1 | −1.3 | 6.7 | −7.3 |
| 500 | 17.1 | −4.4 | 0.2 | 3.6 | −7.4 | 1.5 | 1.4 | 1.3 | −4.7 | −0.9 | 4.8 | 1.6 | 6.6 | 1.2 |
| 850 | −0.1 | 0:9 | −0.2 | −0.1 | 1.2 | −2.8 | 4.5 | 6.2 | −0.6 | 0.2 | 2.4 | 1.4 | 4.8 | 4.5 |

upper troposphere and to dissipate it in the lower troposphere in addition to all the other synoptic-scale processes previously discussed.

The corresponding vertical profiles for the cyclone region shown in Fig. 14 are also in agreement with the results of Reed and Johnson (1974) for composite easterly wave troughs. Given the considerable convective activity that prevailed in the region as deduced from surface, radar and satellite reports, the vertical transport process due to convective-scale motions must be considered a possible mechanism for the apparent vorticity sources and sinks in the upper and lower troposphere. Daggupaty and Sikka (1977) and Shapiro (1978), in addition to Reed and Johnson (1974) and Holton and Colton (1972), have discussed this for tropical systems. The results here are strongly suggestive that the same mechanism is operative in extratropical systems containing significant embedded convective activity.

An additional perspective on the vorticity and kinetic energy structure of the composite anticyclone couplet reported on here and in CB can be drawn from a comparison of some of the published work on the Air Mass Transformation Experiment (AMTEX). The most relevant comparisons would involve the anticyclone region of the present study, a region that encompasses the polar outbreak. Differences in horizontal scale, geography and topography would argue against more than a casual comparison, however.

The results from Kung (1977), Ninomiya (1976a,b) and Fein (1975) reveal the dominance of kinetic energy generation accompanied by considerable horizontal kinetic energy export in the upper troposphere. Very strong downwind transport of kinetic energy from the upper to lower troposphere is also indicated together with a large positive residual in the mid-troposphere. The individual terms in the kinetic energy budget are greater during AMTEX 75 a period noted for numerous cold air outbreaks.

In the anticyclone region of our studies, however, the generation term is of opposite sign, the vertical flux term is of the same sign but vastly reduced in magnitude and the export term is comparable to the AMTEX kinetic energy budget. Poor agreement is found, however, with the $-5$ W m$^{-2}$ generation found by Ninomiya (1976b) for the anticyclonic branch of the polar outbreak over the western AMTEX region.

The corresponding vorticity budget for AMTEX 75 shows the influence of powerful unbalanced cyclonic vorticity advection in the upper troposphere requiring some subsynoptic-scale process which can remove this positive relative vorticity.

Fein (1975) found strong unbalanced cyclonic vorticity advection in the mean over the AMTEX area, whereas advection contributes in the anticyclonic sense over the eastern half of our anticyclone domain.

## 5. Conclusions

A composite cyclone-anticyclone couplet is constructed from four synoptically similar cases of polar air penetration into the Caribbean from off the North American continent. Computations of the relative vorticity and vertical velocity fields along with a vorticity budget equation were carried out for both the upstream polar anticyclone and downstream cyclone in a quasi-Lagrangian coordinate system.

The distributions of the vorticity and vertical velocity in this composite case are comparable to those in a typical midlatitude quasi-geostrophic baroclinic system.

From the computed vorticity budget, it has been shown that the divergence and twisting terms in the lower troposphere, the horizontal advection term in the middle troposphere, and the horizontal, vertical and system advection terms in the upper troposphere provide the negative vorticity tendencies in the area toward which the anticyclone is moving. On the other hand, the divergence term in the lower troposphere and horizontal advection term in the mid and upper troposphere are primarily responsible for the intensification and movement of the downstream cyclone. These are in agreement with what would be expected in an individual midlatitude anticyclone or cyclone.

The most interesting and significant result of the anticyclone vorticity budget is the anticyclonic vorticity depletion in the middle and upper troposphere and corresponding generation in the lower troposphere due to large-scale processes. Consequently, an apparent anticyclonic vorticity source in the middle and upper troposphere and sink in the lower troposphere are required to satisfy the vorticity balance. The result is most likely achieved through subgrid-scale processes.

The corresponding budget for the cyclone region requires an apparent cyclonic vorticity sink in the lower troposphere and source in the mid and upper troposphere for balance. Subgrid-scale convective transport is a possible physical process that can account for this observation.

## REFERENCES

Chen, T-J., and L. F. Bosart, 1977: Quasi-Lagrangian kinetic energy budget of composite cyclone-anticyclone couplets. *J. Atmos. Sci.*, **34**, 452–464.

Daggupaty, S. M., and D. R. Sikka, 1977: On the vorticity budget and vertical velocity distribution associated with the life cycle of a monsoon depression. *J. Atmos. Sci.*, **34**, 773–792.

Fein, J. S., 1975: Vorticity budgets during AMTEX. Management Committee for AMTEX, Sci. Rep., *Fourth AMTEX Study Conf.*, Tokyo.

Holopainen, E. O., 1963: On the dissipation of kinetic energy in the atmosphere. *Tellus*, **15**, 26–32.

——, 1973: An attempt to determine the effects of turbulent friction in the upper troposphere from the balance requirements of the large-scale flow: A frustrating experiment. *Geophysica*, **12**, 151–176.

Holton, J. R., and D. E. Colton, 1972: A diagnostic study of the vorticity balance at 200 mb in the tropics during the northern summer. *J. Atmos. Sci.*, **29**, 1124–1128.

Kung, E. C., 1977: Large-scale energy transformations in the intense winter monsoon over the Kuroshio region. *J. Meteor. Soc. Japan*, **55**, 498–510.

——, and W. E. Baker, 1975: Energy transformations in middle-latitude disturbances. *Quart. J. Roy. Meteor. Soc.*, **101**, 793–815.

Kurihara, Y., 1961: Accuracy of winds aloft data and estimation of error in numerical analysis of atmospheric motions. *J. Meteor. Soc. Japan*, **39**, 331–345.

Ninomiya, K., 1976a: Note on synoptic situation of AMTEX '75. *J. Meteor. Soc. Japan* (Ser., II), **54**, 334–337.

——, 1976b: Wind profile and kinetic energy budget in the mixed layer of a polar air-mass transformed over the Kuroshio region. *J. Meteor. Soc. Japan* (Ser. II), **54**, 361–369.

Reed, R. J., and R. H. Johnson, 1974: The vorticity budget of synoptic-scale wave disturbances in the tropical western Pacific. *J. Atmos. Sci.*, **31**, 1784–1790.

Shapiro, L. J., 1978: The vorticity budget of a composite African tropical wave disturbance. *Mon. Wea. Rev.*, **106**, 806–817.

Smith, P. J., 1973: The kinetic energy budget over North America during a period of major cyclone development. *Tellus*, **25**, 411–423.

Vincent, D. G., W. R. Gommel and L. N. Chang, 1974: Kinetic energy study of Hurricane Celia, 1970. *Mon. Wea. Rev.*, **102**, 35–47.